Available online at www.sciencedirect.com

ScienceDirect

Mendeleev Commun., 2017, **27**, 631–633

Mendeleev Communications

Combustion and passivation of nickel nanoparticles

Michail I. Alymov,[a] Nikolai M. Rubtsov,*[a] Boris S. Seplyarskii,[a] Roman A. Kochetkov,[a] Victor A. Zelensky[b] and Alexey B. Ankudinov[b]

[a] *Institute of Structural Macrokinetics and Materials Science, Russian Academy of Sciences, 142432 Chernogolovka, Moscow Region, Russian Federation. Fax: +7 495 962 8025; e-mail: nmrubtss@mail.ru*

[b] *A. A. Baikov Institute of Metallurgy and Materials Science, Russian Academy of Sciences, 119991 Moscow, Russian Federation*

DOI: 10.1016/j.mencom.2017.11.032

Nanoscaled pyrophoric nickel powders were synthesized by the decomposition of nickel formate layers 1–3 mm thick in a flow of hydrogen at 209 °C and then passivated in a flow of 0.6% oxygen + Ar for 2–10 min. The time of completion of passivation coincides with the time of beginning of cooling down of the sample during passivation.

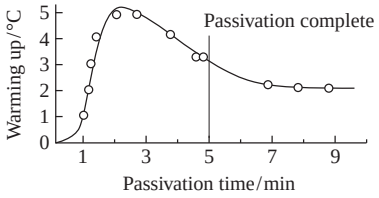

In the past two decades, attention has been focused on the synthesis of metal nanoparticles because of their unusual properties and potential applications in optical, electronic, catalytic and magnetic materials.[1] The physical and chemical properties of Ni, Co and Fe metal nanoparticles depend on particle size and shape.[1–10] Nickel nanomaterials have been synthesized in various forms like nanotubes, nanorods, and hollow spheres.[1,2] Magnetic nanoparticles are widely used in rechargeable batteries,[3] optoelectronics,[4] chemical catalysts,[5,6] drug delivery systems[7] and magnetic hyperthermia.[8] Nickel nanoparticles have a wide range of applications in permanent magnets, magnetic fluids, magnetic recording media, solar energy absorption systems, fuel cell electrodes, catalysts, *etc*.

The methods of the synthesis of particles with controlled size and shape include photolytic and radiolytic reduction,[9] sonochemical methods, solvent extraction reduction, microemulsion technique, polyol process, and chemical route.[2] Nickel nanoparticles are usually prepared in organic media to avoid the formation of nickel oxide or hydroxide, as it takes place in a gas. These can be reduced in a hydrogen flow for more than a day at low temperatures.[10] At higher temperatures, fast coagulation processes lead to the undesirable growth of particles.[2,10] Nickel nanoparticles are pyrophoric.[11] For the further processing of nanopowders in ambient air, they should be either stored in an inert liquid or protected (passivated). The passivation includes in the formation of protective thin oxide or nitride[12] films on the surface of nanoparticles, which prevent the oxidation of metal powders.

Hence, the aim of this work was to synthesize Ni nanoparticles by a chemical metallurgy method and to establish the conditions of their further passivation to prevent oxidation. The synthesized Ni nanopowders were characterized.

The synthesis of nickel formate includes a reaction between nickel sulfate and sodium formate[13] or the direct reaction of basic nickel carbonate[14] or nickel hydroxide with formic acid (the latter was used in this work). Nickel formate dihydrate undergoes dehydration at ~140 °C and decomposition at ~210 °C to give a finely divided Ni powder with the evolution of a gas mixture of carbon dioxide, hydrogen and water[15] by the following reactions:[16,†]

$$Ni(HCOO)_2 \cdot 2H_2O \rightarrow Ni + 2CO_2 + H_2 + 2H_2O, \quad (1)$$

$$Ni(HCOO)_2 \cdot 2H_2O \rightarrow Ni + CO + CO_2 + 3H_2O. \quad (2)$$

† A reactor, which was described elsewhere,[17,18] with nickel formate powder samples 1, 2 and 3 mm thick in a quartz trough was maintained in a furnace at 209 °C for 70 min in a hydrogen flow to reduce either possible NiO formation or CO poisoning of active Ni[19] by reaction (2); then, it was cooled to 20 °C in an argon flow. In some experiments, the reactor with the trough was cooled with ice to 0 °C. The quartz trough was equipped with a chromel–alumel thermocouple (0.2 mm) placed in the powder. Commercial Ni nanoparticles obtained by the electrical explosion of wires were also examined. The mean size of the nanoparticles was 60 nm.

For the passivation of Ni nanopowder, which was performed in the above reactor, 0.6% O_2 was added to an argon flow at 20 °C. The passivation time varied from 2 to 10 min. The detected heating of the thermocouple after O_2 addition indicated the beginning of the passivation. After passivation, the quartz trough with Ni nanopowder was extracted from the reactor and placed on a table for high-speed filming.[17,18] A Casio Exilim F1 PRO color high-speed video camera (60 frames s^{-1} HD) was used to establish the modes of combustion of Ni nanopowder and to control the extent of passivation. A Flir 60 infrared camera (60 frames s^{-1}, 320×240 pix, sensitivity interval of 8–14 μm) was used to determine the dynamics of changes in the sample temperature during combustion.

The phase structure of the samples was studied on a DRON 3M X-ray diffractometer with a coordinate-sensitive detector. The coherent scattering region (CSR) size equal to the mean size of crystallites was also determined. It was 10–15% smaller than the size of small particles (grains) identified using electron microscopy. A CSR size corresponds to the inner ordered region of a grain, and it does not include severely distorted boundaries. The CSR size was calculated by an approximation method applicable to structural components of 20–150 nm in size, which are close to a spherical form and do not have micro tensions; therefore, the size of the objects was underestimated. The BET specific surface areas were measured using a Sorbi-M analyzer.

The microstructure of the powders was examined using a Zeiss Ultra Plus field emission ultra-high resolution scanning electron microscope equipped with an INCA 350 X-ray microanalysis console (Oxford Instruments).

© 2017 Mendeleev Communications. Published by ELSEVIER B.V. on behalf of the N. D. Zelinsky Institute of Organic Chemistry of the Russian Academy of Sciences.

The treatment of nickel formate powder samples in a furnace at 209 °C for 70 min in argon does not lead to the formation of pyrophoric Ni; therefore, the treatment of nickel formate in H_2 instead of Ar prevents either NiO occurrence (NiO is reduced to Ni) or CO poisoning of active Ni (CO reacts with H_2 on active Ni surface).

The results of the speed filming of the combustion of a 2 mm layer of Ni nanopowder without passivation are shown in Figure 1(*a*). The propagating waves of reaction are spatially nonuniform (finger-like[20]). Partially passivated samples also burn in the finger-like mode. Completely passivated powder can also be ignited with a heat source, *e.g.*, a heated wire. The finger-like propagation of a combustion wave initiated with a heated wire in nickel nanopowder (3 mm layer thickness) in air is presented in Figure 1(*b*). This combustion mode is different from the incomplete surface combustion of Fe nanopowder with a pronounced combustion front.[18] Note that the 3 mm thick sample, as distinct from 1 mm thick unpassivated one, never ignited spontaneously, probably, due to heat losses in the bulk of nanopowder. These limiting conditions on the thickness of samples need further investigation. Therefore, the samples 2 mm thick characterized by the phenomena of spontaneous ignition and finger-like combustion were studied.

It is well known that the surface of the charred solid fuel develops fingering patterns resulting from a destabilizing effect of reactant transport.[20,21] Such a scenario was investigated by Zik and Moses.[20] The role of oxygen flow velocity in the observed pattern formation was studied experimentally.[22] Figures 1 and 2 indicate that the 'fingers' occur without any oxidizer flow; *i.e.*, the nature of combustion front instabilities cannot be related to the gas flow. The propagation of 'fingers' in the absence of gas flow is chaotic due to the lack of direction, which is set by the flow. Indeed, under our conditions, the surface of the powder is equally accessible and the external directed gas flow is missing; therefore, the establishment of the driving force that provides finger-like[20]

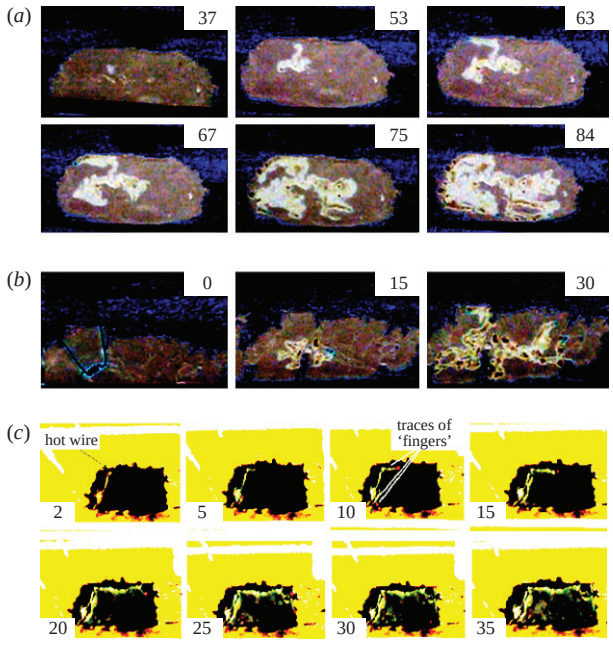

Figure 1 (*a*) Behavior of Ni nanopowder (2 mm thick) in air without passivation, the frame number corresponds to the time (s) after extraction of the trough with nanopowder from the reactor; and initiation of surface combustion of Ni nanopowder in air without passivation (*b*) with a heated wire [3 mm layer thickness, the frame number corresponds to the time (s) after initiation], (*c*) by electro explosion with a heated wire (1 mm layer thickness, initial temperature, 20 °C; 60 frames s^{-1}; the number corresponds to a frame number from the moment of placing the trough on the table; the colors are inverted).

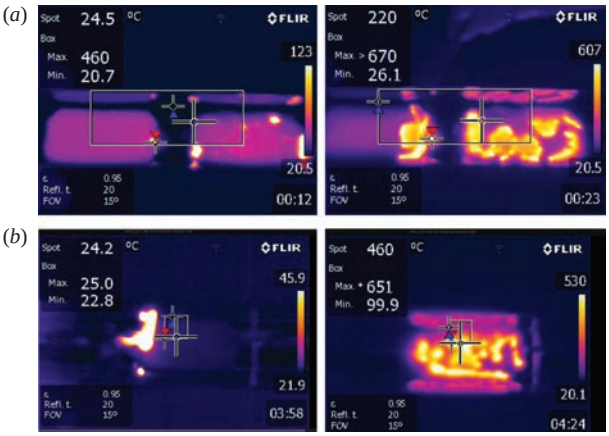

Figure 2 IR investigation of the combustion of Ni nanopowder in air (20 °C without passivation; 60 frames s^{-1}). A bigger cross indicates the temperature in the point, and a smaller cross automatically indicates the maximum temperature over the rectangle in a frame. (*a*) Combustion of Ni nanopowder in air (two samples of 2 mm thick). In the bottom of each frame, to the right the time (s) after extraction of the trough with nanopowder from the reactor is shown. (*b*) Initiation of surface combustion of Ni nanopowder in air with a heated wire (2 mm layer thickness; 5 min passivation).

propagation of reaction waves is quite urgent. The existence of the primary centers of reaction testifies to various chemical activities of different sites of the Ni nanopowder surface [Figure 1(*a*)] as it is observed in Fe nanopowder; this phenomenon can serve as a driving force. On the other hand, the thickness of a reacting layer is determined by the rate of oxygen diffusion through the pores into the bulk of the sample. Therefore, the size and distribution of (nano)pores[23] is a parameter responsible for the propagation of the reaction wave. Anyway, the nature of an inhomogeneous wave in the absence of external flows demands further investigations.[18]

Note that the experiments with layers of Ni nanoparticles obtained by electrical explosion led to similar results, though these particles did not burn spontaneously. This powder can be ignited with an external source [Figure 1(*c*)], and the initiated combustion front also propagated in the form of 'fingers'.

Figure 2 exhibits the IR study of the combustion of Ni nanopowder in air. The frames demonstrate a finger-like character of the combustion of Ni nanopowder. The maximum temperature for the unpassivated sample in the 'tip' of a 'finger' exceeds 670 °C. However, the maximum combustion temperature of the passivated sample does not exceed 651 °C, reflecting the change in heat emission conditions due to a protective oxide layer on nanoparticles.

Figure 3 shows that the maximum warming-up during the passivation with 0.6% O_2 + Ar makes about 5°; the process of passivation comes to an end in ~5 min after the start of 0.6% O_2 + Ar supply, if we determine the moment of completion of passivation as the beginning time point of cooling down of the sample. The Ni samples (2 mm thick) extracted from the reactor burn down completely if the time of passivation is shorter than 3 min. Otherwise, the samples are stable for several weeks, but they can be ignited at any time with a heated wire.

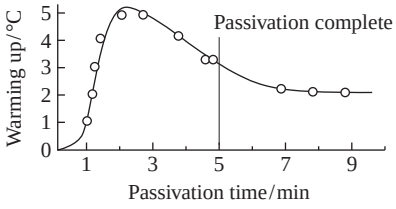

Figure 3 The time dependence of the warming up of the sample 2 mm thick in the process of passivation (T_0 = 20 °C). The vertical solid line indicates the time of passivation completion.

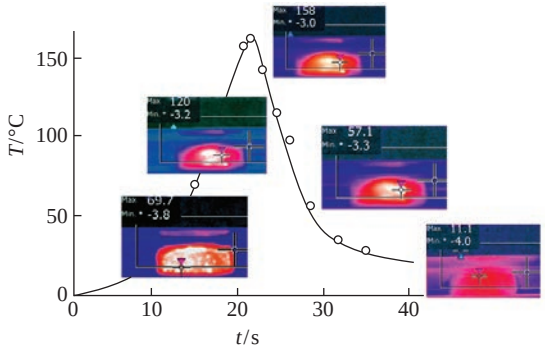

Figure 4 The time dependence of maximum warming up of the sample 2 mm thick without passivation after extraction measured with the IR camera. Initial temperature is –3 °C. Zero time corresponds to the moment of extraction. The corresponding IR video frames are presented. The time of shooting of a frame corresponds to the coordinate of its middle on the abscissa axis.

The appearance of the sample 2 mm thick without passivation cooled down to 0 °C remains the same after extraction from the reactor. The ignition of the sample can be provided with a heated source. Figure 4 shows the time dependence of maximum sample temperature measured with the IR camera, which was 160 °C during passivation in air. At the moment of 10 s, there are several potential centers of combustion in a sample (bright spots), which then disappear; it testifies to various chemical activity of various sites of Ni nanopowder. The warming up at T_0 = 0 °C is due to heat release in Ni oxidation reactions leading to the formation of a thin protective oxide film on the surface of the nanoparticles. Since the ignition does not occur at 0 °C, the rate of heat release becomes smaller than heat losses at a certain moment of passivation,[24] *i.e.* the critical condition of thermal ignition is not attained.

We detected only nickel by the X-ray analysis of the samples 1, 2 and 3 mm thick passivated for 5 min [Figure 5(*a*)]. The CSR size (50–70 nm) was the same for the samples 1, 2 and 3 mm in thickness. As nickel oxides were not detected, an oxide layer was quite thin. This was also supported by the fact that the passivated Ni nanoparticles were not oxidized within several weeks (if the protective film had any defects, or the film was located in any way within the particle, Ni would be fully oxidized).

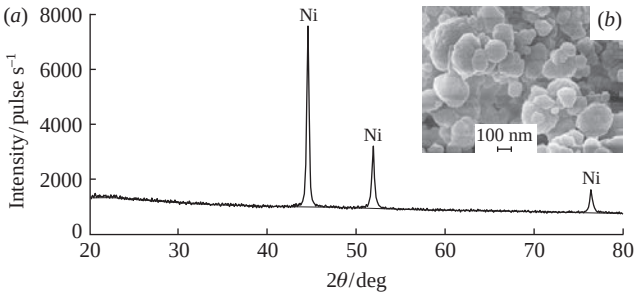

Figure 5 (*a*) The X-ray phase analysis of the passivated Ni nanopowder (5 min in argon containing 0.6% O_2) stored within two weeks, data for sample thicknesses of 1, 2 and 3 mm are identical; (*b*) photo obtained by the scanning electron microscopy of the nickel nanopowder passivated at 20 °C for 10 min in a flow of 0.6% O_2 + Ar.

The determined BET surface areas were 5.2±0.3, 5.7±0.05 and 7.6±0.3 $m^2\ g^{-1}$ for the samples 1, 2 and 3 mm thick, respectively, passivated for 10 min. It meas that the specific surface area and, hence, the size of nanoparticles can be varied by changing the sample thickness. For spherically shaped particles of $d = 6/(rs)$, the mean value of $s = 6.2\ m^2\ g^{-1}$ gives the particle diameter d = 110 nm (r is the density); *i.e.*, the mean particle diameter lies between underestimated (50 nm) and overestimated (110 nm) values. According to Figure 5(*b*), Ni nanoparticles form chains without sealed inner cavities, while the particle diameters were estimated at 50–110 nm.

This work was supported by the Russian Science Foundation (project no. 16-13-00013).

References

1 V. F. Puntes, K. M. Krishnan and A. P. Alivisatos, *Science*, 2001, **291**, 2115.
2 G. Nair and S. Survase, *Int. J. Chem. Phys. Sci*., 2014, **3**, 56.
3 E. Antolini, M. Ferretti and S. Gemme, *J. Mater. Sci*., 1996, **31**, 2187.
4 L. L. Beecroft and C. K. Ober, *Chem. Mater*., 1997, **9**, 1302.
5 A. Yu. Vasil'kov, D. A. Migulin, A. V. Naumkin, O. A. Belyakova, Ya. V. Zubavichus, S. S. Abramchuk, Yu. V. Maksimov, S. V. Novichikhin and A. M. Muzafarov, *Mendeleev Commun*., 2016, **26**, 187.
6 A. A. Shesterkina, O. A. Kirichenko, L. M. Kozlova, G. I. Kapustin, I. V. Mishin, A. A. Strelkova and L. M. Kustov, *Mendeleev Commun*., 2016, **26**, 228.
7 H. T. Zhang, G. Wu, X. H. Chen and X. G. Qiu, *Mater. Res. Bull*., 2006, **41**, 495.
8 M. Bettge, J. Chatterjee and Y. Haik, *BioMagn. Res. Technol*., 2004, **2**, 4.
9 K. Okawa, M. Sekine, M. Maeda, M. Tada, M. Abe, N. Matsushita, K. Nishio and H. Handa, *J. Appl. Phys*., 2006, **99**, 102.
10 D. H. Chen and S. H. Wu, *Chem. Mater*., 2000, **12**, 1354.
11 P. G. Fox, J. Ehretsmann and C. E. Brown, *J. Catal*., 1971, **20**, 67.
12 A. G. Gnedovets, A. B. Ankudinov, V. A. Zelenskii, E. P. Kovalev, H. Wisniewska-Weinert and M. I. Alymov, *Inorg. Mater.: Appl. Res*, 2016, **7**, 303 (*Perspektivnye Materialy*, 2015, no. 12, 62).
13 C. Ellis, *Hydrogenation of Organic Substances*, 3rd edn., D. Van Nostrand Co., New York, 1930.
14 R. Cornubert and C. Borrel, *Bull. Soc. Chim. Fr*., 1930, **47**, 301.
15 J. G. Dean, *Ind. Eng. Chem. Soc*., 1952, **44**, 985.
16 L. L. Bircumshaw and J. Edwards, *J. Chem. Soc*., 1950, 1800.
17 M. I. Alymov, N. M. Rubtsov, B. S. Seplyarskii, V. A. Zelensky and A. B. Ankudinov, *Mendeleev Commun*., 2016, **26**, 452.
18 M. I. Alymov, N. M. Rubtsov, B. S. Seplyarskii, V. A. Zelensky and A. B. Ankudinov, *Mendeleev Commun*., 2016, **26**, 549.
19 V. J. Inglezakis and S. G. Poulopoulos, *Adsorption, Ion Exchange and Catalysis: Design of Operations and Environmental Applications*, Elsevier, Amsterdam, 2006, vol. 3, pp. 490–498.
20 O. Zik and E. Moses, *Phys. Rev. E*, 1999, **60**, 518.
21 L. Kagan and G. Sivashinsky, *Combust. Theory Model*., 2008, **12**, 269.
22 E. R. Ijioma, A. Muntean and T. Ogawa, *Combust. Theory Model*., 2013, **17**, 185.
23 A. B. Yaroslavtsev and Yu. P. Yampolskii, *Mendeleev Commun*., 2014, **24**, 319
24 B. Lewis and G. von Elbe, *Combustion, Flames and Explosions of Gases*, 3rd edn., Academic Press, New York, 1987.

Received: 16th March 2017; Com. 17/5204